Spin-glass state in nickelate superconductors

David R. Saykin,[1,2,3] Martin Gonzalez,[1,4] Jennifer Fowlie,[1,5] Steven A. Kivelson,[3] Harold Y. Hwang,[1,2,5] and Aharon Kapitulnik[1,2,3,5,*]

[1]*Stanford Institute for Materials and Energy Sciences, SLAC National Accelerator Laboratory, 2575 Sand Hill Road, Menlo Park, CA 94025, USA.*
[2]*Geballe Laboratory for Advanced Materials, Stanford University, Stanford, CA 94305, USA.*
[3]*Department of Physics, Stanford University, Stanford, CA 94305, USA.*
[4]*Department of Materials Science and Engineering, Stanford University, Stanford, California 94305, USA.*
[5]*Department of Applied Physics, Stanford University, Stanford, CA 94305, USA.*

(Dated: July 3, 2026)

Magneto-optical measurements in $La_{0.8}Sr_{0.2}NiO_2$ and $Nd_{0.825}Sr_{0.175}NiO_2$ reveal an intriguing new facet of infinite-layer nickelate superconductors: the onset of spin-glass behavior at a temperature far exceeding the superconducting critical temperature T_c. This discovery sharply contrasts with copper oxide superconductors, where magnetism and superconductivity remain largely exclusive. Moreover, the magnitude and onset temperature of the polar Kerr effect in $Nd_{0.825}Sr_{0.175}NiO_2$ fabricated on $SrTiO_3$ and $(LaAlO_3)_{0.3}(Sr_2TaAlO_6)_{0.7}$ substrates differ dramatically, while T_c does not.

INTRODUCTION

It has been a long quest to find a system analogous to the cuprates, in which a parent compound can be doped to reveal high-T_c superconductivity [1]. A typical high-T_c cuprate is characterized by a stack of n-CuO_2 planes each separated by an alkaline-earth element A^{2+} (A=Ca,Sr,Ba) with additional intervening "charge-reservoir" layers that separate the stacks (see e.g. [2]). This structure implies an infinite-layer cuprate structure (where $n \to \infty$) $ACuO_2$ [3], which is a strongly correlated antiferromagnetic charge-transfer insulator [4, 5].

However, its counterpart nickelate system $RNiO_2$ (R = La, Nd, Pr) is either weakly insulating [6] or superconducting [7–9] and lacks long-range antiferromagnetic order [10], while exhibiting a spin-glass behavior [11]. This is despite sharing the same $P4/mmm$ space group and the $3d^9$ configuration in its electronic structure. With the discovery of superconductivity in Sr-doped $NdNiO_2$ with T_c in the range of 9 to 15 K [12], it became clear that the set of a priori expectations for a parent material to exhibit superconductivity needs to be revisited [13].

In many cuprates, doping typically induces a spin-glass (SG) phase, which bridges the loss of antiferromagnetic (AFM) long range order and the emergence of superconductivity (SC) [14]. For example, a thorough study [15] of the magnetic phase diagram of $La_{2-x}Sr_xCuO_4$, a single-layer doped cuprate, revealed that SG order persists far into the superconducting region with a glass transition temperature T_g that is anti-correlated with the superconducting T_c. This is also true for thin films, where the glass transition was shown to be larger, approximately twice as large as the bulk superconducting transition [16]. While T_g seems to diminish towards optimal doping, it seems to show a peak at dopant concentration $x \approx 1/8$, which was previously shown to exhibit a weakened superconducting state. Excluding that last feature, Fig. 1 is the accepted phase diagram for the spin glass phase in cuprates. At low doping ($x \lesssim 2\%$) the transition can be ascribed to freezing of the spins of the doped holes into a SG state which is superimposed on the preexisting 3D AFM long-range order of the Cu^{2+} spins [15–18]. With increased doping ($x \gtrsim 2\%$), stronger frustration of the AFM environment yields a lower-temperature SG phase associated with freezing of spin fluctuations [19–21].

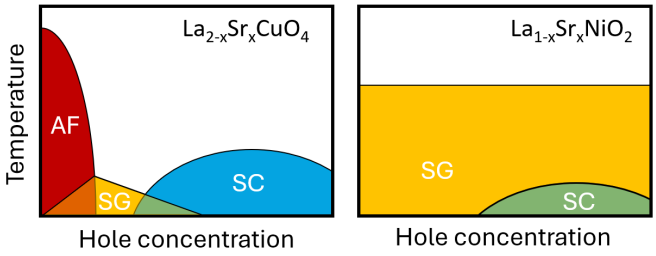

FIG. 1: Schematic phase diagrams showing spin-glass order in cuprates and nickelates. **Left:** The copper oxide superconductor $La_{2-x}Sr_xCuO_4$ exhibits AFM order for $0 \leq x \lesssim 2\%$, and SC for $5\% \lesssim x \lesssim 25\%$. The SG state starts within the AFM phase and apparently leaks into the SC phase [16, 17]. **Right:** Nickelate superconductors have a SG phase that is present in a wide range of Sr doping, such that the SC dome ($10\% \lesssim x \lesssim 25\%$) is located deep inside the SG phase. The exact dependence of SG order on doping concentration is yet to be determined.

While the magnetic structure of infinite-layer nickelate superconductors is yet to be fully understood, particularly as it affects superconductivity, its most salient features are the absence of long–range AFM ordering and freezing of spins into a glass phase even in the parent compound [11, 22, 23]. In the cuprates where magnetism originates from copper spins in the CuO_2 planes, which is also the starting

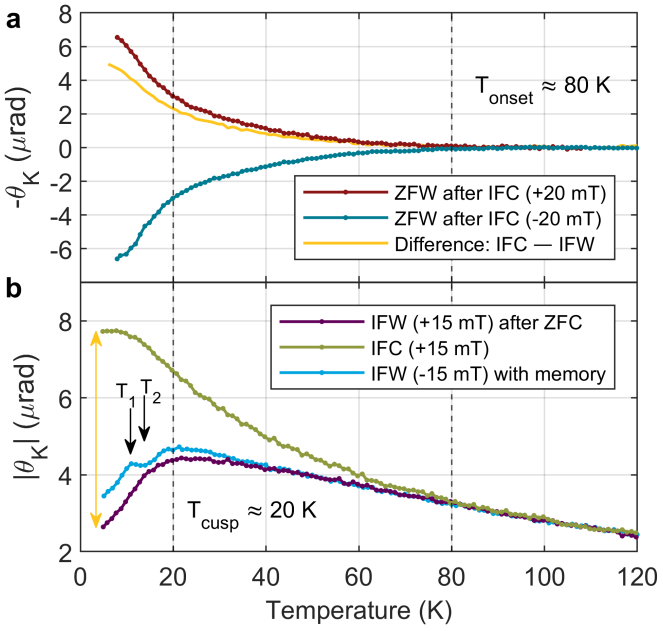

FIG. 2: Kerr signal in $La_{0.8}Sr_{0.2}NiO_2$. Vertical dashed lines indicate the onset temperature $T_{\rm onset}$ and a cusp/peak feature temperature $T_{\rm cusp}$. **a** The Kerr signal recorded in a zero magnetic field warmup (ZFW) after cooling in perpendicular field $B_z = \pm 20$ mT. The difference between IFC in +15 mT and IFW at the same field following a ZFC is shown in yellow. **b** Kerr signal value measured during a warmup in +15 mT after a zero-field cooldown (purple), and during cooldown in same field (green). The cyan curve demonstrates memory effect (see main text).

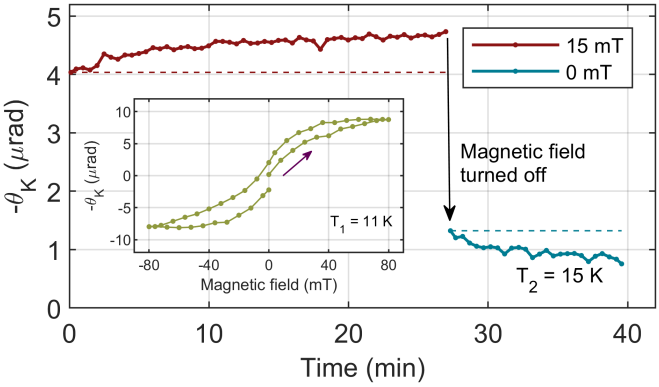

FIG. 3: Slow time saturation and relaxation of magnetization in $La_{0.8}Sr_{0.2}NiO_2$ at $T_2 = 15$ K. The perpendicular magnetic field is abruptly turned on at $t = 0$ and then turned off after $t = 27$ minutes. Horizontal dashed lines are guide for the eye. **Inset:** Hysteresis loop recorded at $T_1 = 11$ K. Arrow indicates the start of the loop. Field was ramped in steps of 8 mT each 30 seconds.

point for models of SG state [24]. By contrast, glassy dynamics observed in polycrystalline $LaNiO_2$ samples were attributed to the presence of subtle local oxygen disorder in the form of remaining apical oxygen [11].

Because superconductivity has so far only been detected in thin films nickelates, their associated magnetic states have not yet been established. A comprehensive muon spin-relaxation (μSR) study of $R_{1-x}Sr_xNiO_2$ by Fowlie *et al.* [25] discovered intrinsic magnetism, which gradually onsets in the 100-150 K temperature range across the rare earth (R) series, and co-exists with superconductivity. These authors speculated that the observed glassy magnetic phase is intrinsic in nature and reflects the AFM coupling between the Ni^+ spins. On the other hand, scanning superconducting quantum interference device (SQUID) microscopy has picked up an inhomogeneous ferromagnetic background in $La_{0.85}Sr_{0.15}NiO_2$ slightly above the superconducting temperature, which has been attributed to extrinsic NiO_x particles on the interface between the nickelate and the $SrTiO_3$ capping layer [26].

Moreover, measurements of the magnetic excitations in $Nd_{1-x}Sr_xNiO_2$ using resonant inelastic x-ray scattering (RIXS) indicate strong spin-1/2 AFM paramagnons [27], while nuclear magnetic resonance (NMR) measurements observe short-range glassy antiferromagnetic fluctuations [28]. These dissimilar observations call for a better understanding of the relationship between magnetism and superconductivity in infinite-layer nickelate superconductors.

In this paper we present a comprehensive study of the magnetic state of doped infinite layer nickelates through highly sensitive measurements of the magneto-optical polar Kerr (MOKE) and Faraday (MOFE) effects using zero area-loop Sagnac interferometers (ZALSI) [29]. Our work provides direct evidence of a spin-glass magnetic state in infinite-layer nickelate superconductors through observations of: *i*) Irreversible magnetic susceptibility, *ii*) Slow dynamics and aging, *iii*) memory effect. Focusing on doping levels close to optimal doping, we further demonstrate the robustness of superconductivity in the presence of a glass phase with $T_g > T_c$.

RESULTS

The detailed design of ZALSI is described in the Methods section and Supplementary Information [30]. Most importantly, the Kerr angle is a direct probe of magnetization since it is proportional to Hall conductivity at the frequency of light [31–33].

$$\theta_K \propto \sigma_{xy}(\omega) \propto \pm M_z \qquad (1)$$

Since time-reversal symmetry breaking is a necessary condition for a finite Kerr effect [34], we will refer to polar Kerr rotation simply as the *magnetic signal*.

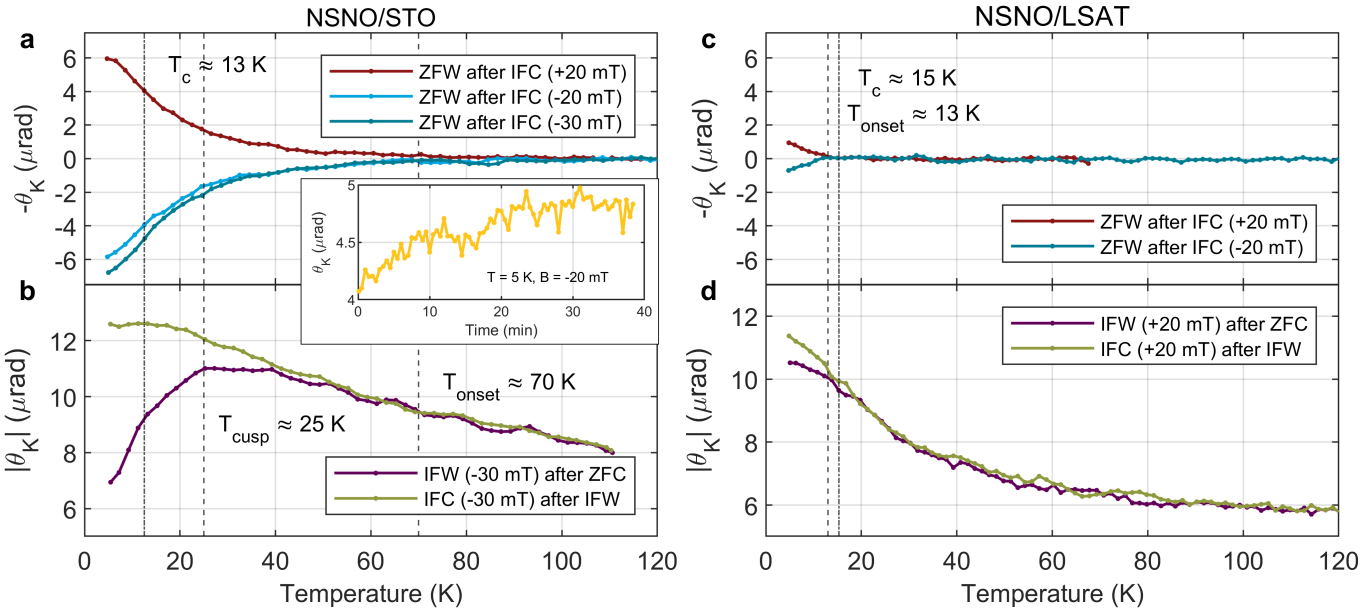

FIG. 4: Kerr signal in $Nd_{0.825}Sr_{0.175}NiO_2$. **a,b** NSNO on STO substrate. **a** Data, taken during a zero-field warm-up (ZFW) preceded by cooldown from 150 K in perpendicular magnetic field. **b** Kerr rotation in nickelate in the presence of −30 mT magnetic field taken during the warmup after zero-field cooldown and during the in-field cooldown. **c,d** NSNO on LSAT substrate. Measurement protocol in **c** and **d** is the same as in **a** and **b** respectively.

Figures 2 and 3 show evidence for spin glass behavior in $La_{0.8}Sr_{0.2}NiO_2$ (LSNO). Figure 2 demonstrates the presence of spontaneous magnetization, which gradually emerges in LSNO below $T_{\text{onset}} \simeq 80$ K. When the sample is field-cooled in a small field of ±20 mT and then the field is turned off at the base temperature $T_{\text{base}} \sim 5$ K, any remanent Kerr rotation is evidence for aligned magnetic moments in the material. Reversing the direction of the training field leads to the reversal of the sign of the Kerr signal, which confirms the magnetic nature of the optical signal. The observed smooth onset of the magnetic signal is characteristic for glassy systems.

In-field cooldown and warmup measurements (bottom panel of Fig. 2) probe magnetic susceptibility, which appears to be irreversible: following a zero-field cooldown (ZFC), magnetic moments are frozen and cannot be rotated by a weak external field, while during the in-field cooldown (IFC), moments are aligned with the field. The difference between these two measured susceptibilities (IFW and IFC) is roughly the same as the remanent magnetization extracted during the measurement with ZFW protocol as shown by the yellow line on the top panel of the Fig. 2 .

Irreversible behavior of magnetic susceptibility and gradual onset of magnetization are known properties of spin-glass; however these could also be explained with domain physics alone. Thus, to verify the SG nature of magnetic state in nickelate superconductors, we further probe dynamical manifestations of SG phase.

After cooling the sample in zero-field from room temperature to T_{base}, we heat it up to $T_2 = 15$ K, turn on a weak external field $B_z = +15$ mT and record Kerr signal as a function of time. As evident from Figure 3, magnetization slowly increases on the scale of minutes; this property of spin-glass is known as *aging*. Once the field is turned off, the magnetization slowly relaxes to some finite but smaller value on a similar time scale. The observed time-dependence of magnetic susceptibility is characteristic of glass-like spin dynamics and is comparable to analogous experiments performed on bulk polycrystalline $LaNiO_2$ samples [11, 22].

From T_2 we cool the sample down to $T_1 = 11$ K and perform a hysteresis loop by sweeping the field to +80 mT, then to −80 mT and back to zero. The resulting hysteresis curve is depicted in the inset of Fig. 3 . Finally, we cool down to a base temperature of $T_0 = 5$ K, turn on an opposite field $B_z = -15$ mT and record the Kerr signal during in-field warmup, which exhibits a relatively sharp, non-monotonic features at $T_1 = 11$ and $T_2 = 15$ K (see Figure 2b). This unusual effect can be explain as a manifestation of the "memory effect," which happens because the systems retains information about spin dynamics that was happening at T_1 and T_2 prior to cooldown. Above T_2 the magnetic susceptibility recovers the same trend that was recorded during the previous in-field warmup after zero-field cooldown. The hierarchic structure of the free-energy landscape with many local minima leads to apparent "memory" about the state from which the system was cooled down [35].

Finally, we direct our attention to measurements

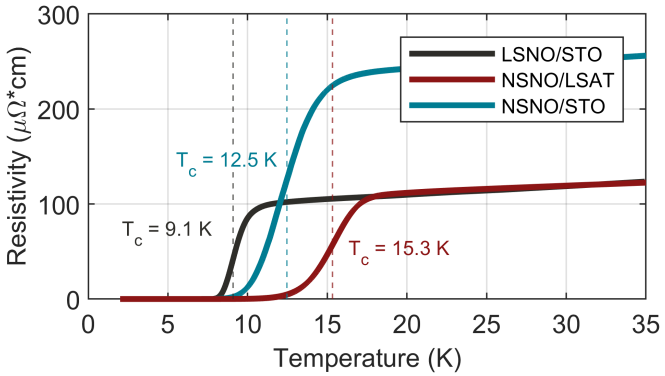

FIG. 5: Resistivity of LSNO, NSNO/STO, and NSNO/LSAT. Superconducting transition temperatures T_c (indicated with dashed lines) were determined as the mean of inflection point temperature and half-normal point temperature.

of $Nd_{0.825}Sr_{0.175}NiO_2$ (NSNO) samples prepared on $SrTiO_3$ and $(LaAlO_3)_{0.3}(Sr_2TaAlO_6)_{0.7}$ substrates, abbreviated as STO and LSAT respectively (Fig. 4). It was shown that nickelate films prepared on LSAT substrate have higher crystallinity compared to the similar films fabricated on STO substrate [36, 37]. This is evident from the reduction in Ruddlesden-Popper-type stacking faults, improved metallicity, and an increase in the superconducting critical temperature (see Fig. 5) when compared to NSNO on STO [38].

The irreversible trend in Kerr susceptibility, together with the aging effect, undoubtedly demonstrates glassy nature of magnetic order in $Nd_{0.825}Sr_{0.175}NiO_2$. Furthermore, the data explicitly demonstrates a significant difference in the strength of magnetic signal between the two NSNO samples grown on different substrates,which we attribute to the difference in films quality as well as strain-epitaxy.

Specifically, the magnitude of the zero-field Kerr signal at base temperature drops from about 6 μrad to about 1 μrad, while onset temperature is decreased to $T_{\text{onset}} \approx 13$ K in NSNO/LSAT sample compared to $T_{\text{onset}} \approx 70$ K in the NSNO/STO. In fact, since full strength of magnetic signal in NSNO/LSAT is just $\theta_K^{(0)} \approx 850$ nanorad (see Fig. 4 c), we're unable to demonstrate aging phenomenon in this sample. Based on the similar measurements in LSNO/STO and NSNO/STO samples, we would expect the aging magnitude $\theta_K(t = 30\text{min}) - \theta_K(t = 0)$ to be an order magnitude smaller then $\theta_K^{(0)}$, which is below the resolution of our apparatus of 100 nanorads. Still, irreversible susceptibility and gradual onset of magnetic signal in zero-field measurements are indicative of a spin-glass state. We also note that in NSNO/LSAT samples we observe only a single characteristic temperature, at which the signal onsets, but we do not see any cusp-type features in the susceptibility data.

DISCUSSION

Our results of the dynamics of the magnetic state of doped thin films nickelates are in good agreement with the magnetic susceptibility measurements of the polycrystalline parent compound $LaNiO_2$ [11, 22], which demonstrated similar hallmarks of SG phase: irreversible susceptibility, aging, and a memory effect. The authors of [11] have also identified two characteristic temperatures associated with SG behavior in the AC susceptibility of $LaNiO_2$: cusp-like peak feature around $T_{\text{cusp}} \simeq 13$ K and an onset of frequency-dependent susceptibility at $T_{\text{onset}} \simeq 85$ K. Approximate typical temperatures are summarized in the Table I. Based on this observation, they surmised the possible existence of two disorder mechanisms at play with different characteristic energy scales.

However, it is challenging to estimate the exact SG emergence temperature due to the gradual nature of the transition, based on T_{cusp} and the magnitude of the splitting between susceptibility curves, magnetic signal in the thin films on the STO substrate appears to be comparable to the signal in the (undoped) nickelate crystals [11], which generally have lower crystallinity [39]. This similarity appears to be even more bizarre, when it is taken into account that polycrystalline samples are reported to have no nickel impurities, while ~ 37 nickel particles per μm^2 have been reported in the thin-film samples [26]. In any case, the onset temperature of the SG phase does not depend strongly on the rare earth ion or Sr doping, which permits us to surmise the phase diagram shown in Fig. 1 .

Importantly, present magneto-optical measurements agree with the μSR study [25], conducted on the same $La_{0.8}Sr_{0.2}NiO_2$ sample as measured in the current work. We speculate that the spin-glass magnetic order detected with ZALSI is responsible for the change in muon spin relaxation rate between $T = 100$ K and $T = 5$ K reported in Ref. [25]. Since μSR confirm the bulk nature of the magnetic signal, we conclude that the glassy spin dynamics is not caused by extrinsic factors such as Ni clusters on the interface with the capping layer, but instead arise due to intrinsic mechanisms. However, in contrast to μSR we can exclude the AFM interaction as the origin of the observed glassy magnetic state, since compensated AFM ordered moments would not produce any Kerr rotation.

Finally we comment on the large reduction in strength and characteristic temperature of the magnetic signal between the NSNO samples that are fabricated on STO and LSAT substrates. A relatively moderate increase by 20 % in superconducting temperature (see Fig. 5), indicates that the mechanism for "static" magnetism in nickelates is weakly related to superconductivity. Instead, it appears that the overall improvement in the sample's crystallinity is responsible for the suppressed SG state. Furthermore, as evident from the RIXS study of $PrNiO_2$, the paramagnon spectrum does not change between sam-

Sample	T_c	$T_{\rm cusp}$	$T_{\rm onset}$
$LaNiO_2$ (polycrystal) [11]	-	13	85
$NdNiO_2$ (polycrystal) [11]	-	6	85
$La_{0.8}Sr_{0.2}NiO_2$ / STO	9.1	20	80
$Nd_{0.825}Sr_{0.175}NiO_2$ / STO	12.5	25	70
$Nd_{0.825}Sr_{0.175}NiO_2$ / LSAT	15.3	-	13

TABLE I: Summary of the transition temperatures (in Kelvins) for different samples: undoped crystalline materials from Ref. [11] and optimally doped superconducting thin films.

ples prepared on STO or LSAT substrates [40].

The main results of the present work are magneto-optical measurements of superconducting infinite-layer nickelates $La_{0.8}Sr_{0.2}NiO_2$ and $Nd_{0.825}Sr_{0.175}NiO_2$, which clearly demonstrate the presence of a spin-glass phase coexisting with superconductivity and persisting up to temperatures T_g much higher than superconducting critical temperature T_c. The dramatic change in magnetic signal and onset temperature between $Nd_{0.825}Sr_{0.175}NiO_2$ samples grown on $SrTiO_3$ and $(LaAlO_3)_{0.3}(Sr_2TaAlO_6)_{0.7}$ substrates indicates the importance of the sample's crystallinity on the disorder magnitude in the exchange interaction energy. On the other hand, the relatively smaller effect this change has on the superconducting T_c suggests that there is no simple, direct connection between SG order and the mechanism of superconductivity in this material - and possibly, by analogy - in the cuprates as well.

METHODS

The ZALSI apparatus has a unique symmetry-based design that enables the measurement of the Kerr angle θ_K with sub-microradian resolution. ZALSI has been used to detect time-reversal symmetry breaking (TRSB) in superconductors [41–45] and thin film ferromagnets [46]. It was recently demonstrated that ZALSI is sensitive exclusively to TRSB and does not suffer from optical activity induced by non-magnetic phases such as charge order [47–49].

We use continuous superluminescent diode light source operating at $\lambda = 1550$ nm SLED, which corresponds to $\omega \simeq 0.8$ eV. Additionally, we have repeated selected measurements with 830 nm (1.5 eV) ZALSI, and found qualitatively similar results. Notably, the Kerr rotation from the LSNO at 830 nm is reversed in sign and has a smaller magnitude compared to signal detected at 1550 nm.

$$\theta_K^{\lambda=830\text{ nm}} \propto +M_z, \tag{2}$$

$$\theta_K^{\lambda=1550\text{ nm}} \propto -M_z. \tag{3}$$

This behavior is, in fact, similar to elemental nickel, where Kerr angle is known to reverse sign at $\omega \approx 1$ eV [50]. Moreover, for in-field measurements paramagnetic-like contributions from the substrate is much larger at 830 nm. This makes longer wavelengths more suitable for studying magnetism in nickelate superconductors.

Overall, magneto-optical Kerr effect measurements are perfectly suited for studying magnetization in nickelate thin-film superconductors, since they allow for local bulk probe (beam spot size ≈ 25 μm) of magnetization in a wide range of temperatures. However, due to tiny absolute magnitude of the SG signal of ~ 5 μrad, this measurement is beyond the reach of conventional MOKE setups, whereas ZALSI is able to resolve such signals with ease owing to its extremely high sensitivity of 100 nrad/$\sqrt{\text{Hz}}$. See the Supplementary Material [30] for more details on relationship between ZALSI MOKE signal and magnetization, its dependence on wavelength, and substrate contributions.

Acknowledgments

We thank Daniel S. Fisher for the insightful discussions. This work at Stanford University was supported by the U.S. Department of Energy, Office of Science, Basic Energy Sciences, Division of Materials Sciences and Engineering, under Contract DE-AC02-76SF00515.

* aharonk@stanford.edu

[1] B. Keimer, S. A. Kivelson, M. R. Norman, S. Uchida, and J. Zaanen, Nature **518**, 179 (2015).

[2] C. Park and R. L. Snyder, Journal of the American Ceramic Society **78**, 3171 (1995), https://ceramics.onlinelibrary.wiley.com/doi/pdf/10.1111/j.1151-2916.1995.tb07953.x.

[3] T. Siegrist, S. M. Zahurak, D. W. Murphy, and R. S. Roth, Nature **334**, 231 (1988).

[4] D. Vaknin, E. Caignol, P. K. Davies, J. E. Fischer, D. C. Johnston, and D. P. Goshorn, Phys. Rev. B **39**, 9122 (1989).

[5] R. T. Scalettar, D. J. Scalapino, R. L. Sugar, and S. R. White, Phys. Rev. B **44**, 770 (1991).

[6] A. Ikeda, T. Manabe, and M. Naito, Physica C: Superconductivity **495**, 134 (2013).

[7] M. Osada, B. Y. Wang, B. H. Goodge, S. P. Harvey, K. Lee, D. Li, L. F. Kourkoutis, and H. Y. Hwang, Advanced Materials **33**, 2104083 (2021), https://advanced.onlinelibrary.wiley.com/doi/pdf/10.1002/adma.2021

[8] C. Parzyck, Y. Wu, L. Bhatt, M. Kang, Z. Arthur, T. Pedersen, R. Sutarto, S. Fan, J. Pelliciari, V. Bisogni, *et al.*, arXiv preprint arXiv:2410.02007 (2024).

[9] H. Sahib, A. Raji, F. Rosa, G. Merzoni, G. Ghiringhelli, M. Salluzzo, A. Gloter, N. Viart, and D. Preziosi, Advanced Materials , 2416187 (2024).

[10] M. Hayward and M. Rosseinsky, Solid State Sciences **5**, 839 (2003), international Conference on Inorganic Materials 2002.

[11] H. Lin, D. J. Gawryluk, Y. M. Klein, S. Huangfu, E. Pomjakushina, F. von Rohr, and A. Schilling, New Journal of Physics **24**, 013022 (2022).

[12] D. Li, K. Lee, B. Y. Wang, M. Osada, S. Crossley, H. R. Lee, Y. Cui, Y. Hikita, and H. Y. Hwang, Nature **572**, 624 (2019).

[13] A. S. Botana and M. R. Norman, Phys. Rev. X **10**, 011024 (2020).

[14] A. Aharony, R. J. Birgeneau, A. Coniglio, M. A. Kastner, and H. E. Stanley, Phys. Rev. Lett. **60**, 1330 (1988).

[15] M.-H. Julien, Physica B: Condensed Matter **329-333**, 693 (2003), proceedings of the 23rd International Conference on Low Temperature Physics.

[16] E. Stilp, A. Suter, T. Prokscha, E. Morenzoni, H. Keller, B. M. Wojek, H. Luetkens, A. Gozar, G. Logvenov, and I. Božović, Phys. Rev. B **88**, 064419 (2013).

[17] C. Niedermayer, C. Bernhard, T. Blasius, A. Golnik, A. Moodenbaugh, and J. I. Budnick, Phys. Rev. Lett. **80**, 3843 (1998).

[18] J. L. Tallon, C. Bernhard, and C. Niedermayer, Superconductor Science and Technology **10**, A38 (1997).

[19] F. C. Chou, N. R. Belk, M. A. Kastner, R. J. Birgeneau, and A. Aharony, Phys. Rev. Lett. **75**, 2204 (1995).

[20] N. Hasselmann, A. H. Castro Neto, and C. Morais Smith, Phys. Rev. B **69**, 014424 (2004).

[21] B. M. Andersen, M. Schmid, S. Graser, P. Hirschfeld, and A. P. Kampf, Journal of Physics and Chemistry of Solids **72**, 358 (2011), spectroscopies in Novel Superconductors 2010.

[22] R. A. Ortiz, P. Puphal, M. Klett, F. Hotz, R. K. Kremer, H. Trepka, M. Hemmida, H.-A. K. von Nidda, M. Isobe, R. Khasanov, H. Luetkens, P. Hansmann, B. Keimer, T. Schäfer, and M. Hepting, Phys. Rev. Res. **4**, 023093 (2022).

[23] P. Puphal, B. Wehinger, J. Nuss, K. Küster, U. Starke, G. Garbarino, B. Keimer, M. Isobe, and M. Hepting, Phys. Rev. Mater. **7**, 014804 (2023).

[24] P. Werner and S. Hoshino, Phys. Rev. B **101**, 041104 (2020).

[25] J. Fowlie, M. Hadjimichael, M. M. Martins, D. Li, M. Osada, B. Y. Wang, K. Lee, Y. Lee, Z. Salman, T. Prokscha, *et al.*, Nature Physics **18**, 1043 (2022).

[26] R. A. Shi, B. Y. Wang, Y. Iguchi, M. Osada, K. Lee, B. H. Goodge, L. F. Kourkoutis, H. Y. Hwang, and K. A. Moler, Physical Review Materials **8**, 024802 (2024).

[27] H. Lu, M. Rossi, A. Nag, M. Osada, D. F. Li, K. Lee, B. Y. Wang, M. Garcia-Fernandez, S. Agrestini, Z. X. Shen, E. M. Been, B. Moritz, T. P. Devereaux, J. Zaanen, H. Y. Hwang, K.-J. Zhou, and W. S. Lee, Science **373**, 213 (2021), https://www.science.org/doi/pdf/10.1126/science.abd7726.

[28] Y. Cui, C. Li, Q. Li, X. Zhu, Z. Hu, Y.-f. Yang, J. Zhang, R. Yu, H.-H. Wen, and W. Yu, Chinese Physics Letters **38**, 067401 (2021).

[29] J. Xia, P. T. Beyersdorf, M. M. Fejer, and A. Kapitulnik, Applied Physics Letters **89**, 062508 (2006).

[30] "Supplementary material," URL will be provided by publisher. It includes Refs. [25, 29, 31, 34, 36, 41, 43–45, 47, 48, 51].

[31] P. M. Oppeneer, *Theory of the magneto-optical Kerr effect in ferromagnetic compounds*, Ph.D. thesis (1999).

[32] A. Kapitulnik, Physica B: Condensed Matter **460**, 151 (2015), special Issue on Electronic Crystals (ECRYS-2014).

[33] A. D. Fried, Physical Review B **90**, 121112 (2014).

[34] B. I. Halperin, in *The Physics and Chemistry of Oxide Superconductors*, edited by Y. Iye and H. Yasuoka (Springer Berlin Heidelberg, Berlin, Heidelberg, 1992) pp. 439–450.

[35] V. S. Dotsenko, Uspekhi Fizicheskikh Nauk **163**, 1 (1993).

[36] K. Lee, B. Y. Wang, M. Osada, B. H. Goodge, T. C. Wang, Y. Lee, S. Harvey, W. J. Kim, Y. Yu, C. Murthy, S. Raghu, L. F. Kourkoutis, and H. Y. Hwang, Nature **619**, 288 (2023).

[37] X. Ren, J. Li, W.-C. Chen, Q. Gao, J. J. Sanchez, J. Hales, H. Luo, F. Rodolakis, J. L. McChesney, T. Xiang, *et al.*, Communications Physics **6**, 341 (2023).

[38] K. Lee, B. H. Goodge, D. Li, M. Osada, B. Y. Wang, Y. Cui, L. F. Kourkoutis, and H. Y. Hwang, APL Materials **8**, 041107 (2020), https://pubs.aip.org/aip/apm/article-pdf/doi/10.1063/5.0005103/14564406/041107_1_online.pdf.

[39] Q. Li, C. He, J. Si, X. Zhu, Y. Zhang, and H.-H. Wen, Communications Materials **1**, 16 (2020).

[40] Q. Gao, S. Fan, Q. Wang, J. Li, X. Ren, I. Biało, A. Drewanowski, P. Rothenbühler, J. Choi, R. Sutarto, *et al.*, Nature Communications **15**, 5576 (2024).

[41] J. Xia, Y. Maeno, P. T. Beyersdorf, M. M. Fejer, and A. Kapitulnik, Phys. Rev. Lett. **97**, 167002 (2006).

[42] J. Xia, V. Shelukhin, M. Karpovski, A. Kapitulnik, and A. Palevski, Phys. Rev. Lett. **102**, 087004 (2009).

[43] E. R. Schemm, W. J. Gannon, C. M. Wishne, W. P. Halperin, and A. Kapitulnik, Science **345**, 190 (2014).

[44] I. M. Hayes, D. S. Wei, T. Metz, J. Zhang, Y. S. Eo, S. Ran, S. R. Saha, J. Collini, N. P. Butch, D. F. Agterberg, A. Kapitulnik, and J. Paglione, Science **373**, 797 (2021).

[45] D. S. Wei, D. Saykin, O. Y. Miller, S. Ran, S. R. Saha, D. F. Agterberg, J. Schmalian, N. P. Butch, J. Paglione, and A. Kapitulnik, Phys. Rev. B **105**, 024521 (2022).

[46] J. Xia, W. Siemons, G. Koster, M. R. Beasley, and A. Kapitulnik, Phys. Rev. B **79**, 140407(R) (2009).

[47] D. R. Saykin, C. Farhang, E. D. Kountz, D. Chen, B. R. Ortiz, C. Shekhar, C. Felser, S. D. Wilson, R. Thomale, J. Xia, and A. Kapitulnik, Phys. Rev. Lett. **131**, 016901 (2023).

[48] C. Farhang, J. Wang, B. R. Ortiz, S. D. Wilson, and J. Xia, Nature Communications **14**, 5326 (2023).

[49] C. Farhang, W. R. Meier, W. Lu, J. Li, Y. Wu, S. Mozaffari, R. P. Madhogaria, Y. Zhang, D. Mandrus, and J. Xia, arXiv preprint arXiv:2502.14568 (2025).

[50] K. Buschow, Handbook of Ferromagnetic Materials, **4**, 493 (1988).

[51] L. D. Landau, J. S. Bell, M. Kearsley, L. Pitaevskii, E. Lifshitz, and J. Sykes, *Electrodynamics of continuous media*, Vol. 8 (elsevier, 2013).